Biometrics, Impact, and Significance of Basal Linear Deposit and Subretinal Drusenoid Deposit in Age-Related Macular Degeneration

Ling Chen,[1,2] Jeffrey D. Messinger,[2] Deepayan Kar,[2] Jacque L. Duncan,[3] and Christine A. Curcio[2]

[1]The First Affiliated Hospital of Chongqing Medical University, Chongqing Key Laboratory of Ophthalmology, and Chongqing Eye Institute, Chongqing, China
[2]Department of Ophthalmology and Visual Sciences, School of Medicine, University of Alabama at Birmingham, Birmingham, Alabama, United States
[3]Department of Ophthalmology, University of California San Francisco, San Francisco, California, United States

Correspondence: Christine A. Curcio, Department of Ophthalmology and Visual Sciences, EyeSight Foundation of Alabama Vision Research Laboratories, 1670 University Boulevard Room 360, University of Alabama at Birmingham School of Medicine, Birmingham, AL 35294-0019, USA; christinecurcio@uabmc.edu.

Received: November 25, 2020
Accepted: January 4, 2021
Published: January 29, 2021

Citation: Chen L, Messinger JD, Kar D, Duncan JL, Curcio CA. Biometrics, impact, and significance of basal linear deposit and subretinal drusenoid deposit in age-related macular degeneration. *Invest Ophthalmol Vis Sci.* 2021;62(1):33. https://doi.org/10.1167/iovs.62.1.33

Purpose. Basal linear deposit (BLinD) is a thin layer of soft drusen material. To elucidate the biology of extracellular deposits conferring age-related macular degeneration (AMD) progression risk and inform multimodal clinical imaging based on optical coherence tomography (OCT), we examined lipid content and regional prevalence of BLinD, soft drusen, pre-BLinD, and subretinal drusenoid deposit (SDD) in AMD and non-AMD aged eyes. We estimated BLinD volume and illustrated its relation to type 1 macular neovascularization (MNV).

Methods. Donor eyes were classified as early to intermediate AMD ($n = 25$) and age-matched controls ($n = 54$). In high-resolution histology, we assessed BLinD/soft drusen thickness at 836 and 1716 locations in AMD and control eyes, respectively. BLinD volume was estimated using solid geometry in donor eyes, one clinically characterized.

Results. BLinD, drusen, type 1 MNV, and fluid occupy the sub-RPE-basal laminar space. BLinD volume in a 3-mm diameter circle may be as much as 0.0315 mm^3. Osmophilic lipid was more concentrated in BLinD/drusen than SDD. In the fovea, BLinD/drusen was prevalent in AMD eyes; pre-BLinD was prevalent in control eyes. SDD was low in the fovea and high in perifovea, especially in AMD eyes.

Conclusions. Although invisible, BLinD may presage type 1 MNV. BLinD volume approaches the criterion OCT drusen volume of 0.03 mm^3 for AMD progression risk. BLinD culminates years of subfoveal lipid accumulation. SDD is detected relatively late in life, with currently unknown precursors. Deposit topography suggests one outer retinal lipid recycling system serving specialized cone and rod physiology, and its dysregulation in AMD is due to impaired transfer to the circulation.

Keywords: age-related macular degeneration, basal linear deposit, clinicopathologic correlation, drusen, histopathology, histology, neovascularization, optical coherence tomography, photoreceptors, subretinal drusenoid deposit

Age-related macular degeneration (AMD) is the fourth largest cause of vision loss globally[1] due to macular neovascularization (MNV) and macular atrophy (MA) in its advanced forms. Extracellular deposits called drusen are the major intraocular risk factor for AMD progression in longitudinal studies using color fundus photography.[2–4] Soft drusen concentrated under the fovea confer a remarkably high risk for MNV or MA, with a relative risk at 10 years of 26.5 for baseline drusen in the central 1-mm diameter.[3] New understanding of drusen composition has motivated the therapeutic targeting of lipids, a major druse component.[5–8] More data about drusen biology could help inform effective measures to prevent MNV and MA altogether.

Soft drusen and basal linear deposit (BLinD) are lump-and-layer versions of the same lipid-rich extracellular material.[9,10] This material localizes between the basal lamina of the retinal pigment epithelium (RPE-BL) and the inner collagenous layer (ICL) of Bruch's membrane (BrM) (Fig. 1). The principal component was called membranous debris and correlated to clinically visible soft drusen by Sarks et al.[9,11] Much evidence indicates that membranous debris is partially preserved lipoproteins of retinal pigment epithelium (RPE) origin, similar in size to plasma very low-density lipoproteins.[10,12] Enrichment with esterified cholesterol and the fatty acid linoleate suggests major sources of photoreceptor outer segments and diet, respectively.[13,14]

Optical coherence tomography (OCT) is widely used to evaluate and manage AMD and reveal the three-dimensional microstructure of MNV and MA precursors. In consensus nomenclature, the fourth outer retinal hyperreflective band

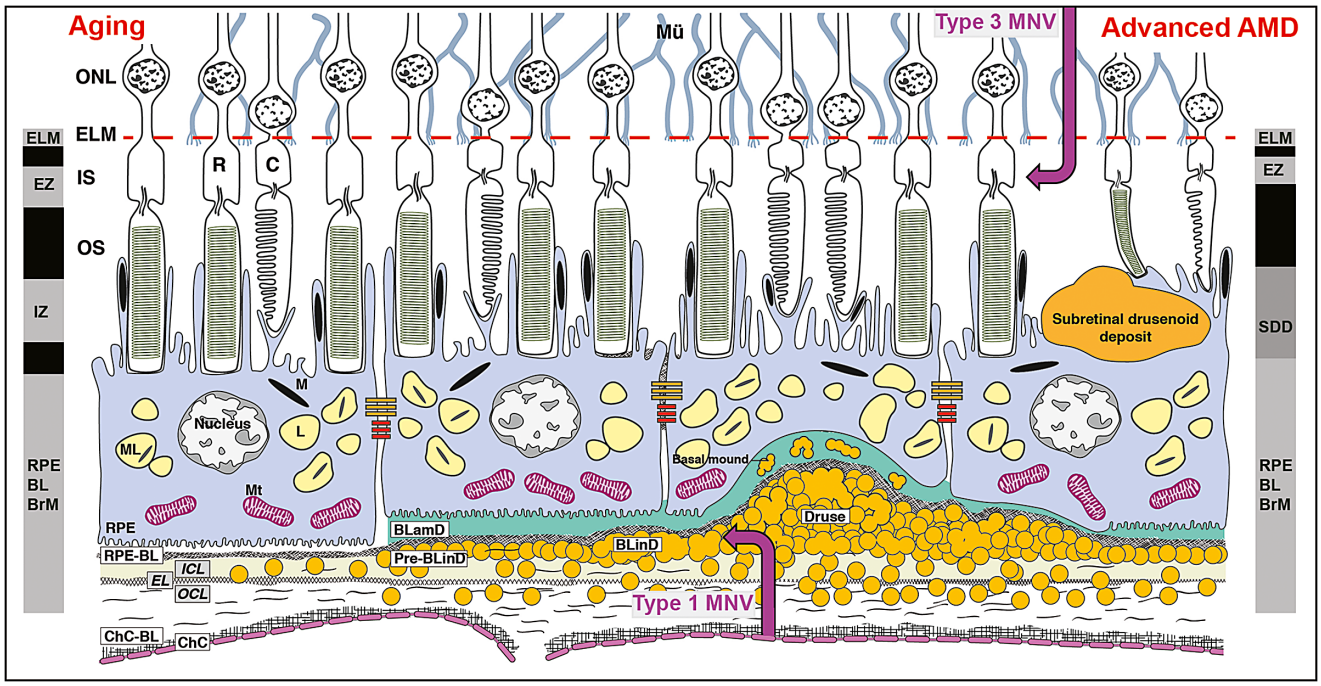

Figure 1. The layers of age-related macular degeneration and outer retinal hyperreflective bands of optical coherence tomography. The vertical dimension is expanded to highlight thin anatomic layers between outer segments and choriocapillaris and incorporated into the fourth outer retinal hyperreflective band of OCT. The trilaminar BrM[18] consists of inner collagenous (ICL), elastic (EL), and outer collagenous (OCL) layers. The RPE as an epithelium rests on a basal lamina (BL) of extracellular matrix (at *left*).[15] BLamD is a stereotypically thickened extracellular matrix (*green*, in *middle* and *right*) between the RPE plasma membrane and RPE-BL, either replacing or incorporating infoldings of basal RPE. Between the RPE-BL or BLamD and ICL of BrM is the sub-RPE-BL space. In this space accumulates soft drusen material[9] and, in some eyes, type 1 MNV of choroidal origin (*up-arrow*), with sequelae of fluid, cells, and fibrosis. Soft druse material is found also in BLinD and in basal mounds within BLamD.[103] BLinD may be continuous with, yet distinct from, dome-shaped drusen. Between the RPE and photoreceptors are SDDs (first called reticular pseudodrusen), extracellular material that is reflective on OCT and directly disruptive to photoreceptors.[104] Eyes with SDDs are at risk for type 3 MNV (*down-arrow*)[105,106] of retinal origin (called retinal angiomatous proliferation).[107] The vertical bars show the third and fourth outer retinal hyperreflective bands of currently available spectral domain OCT,[15] with our interpretations.[18] The third band, called the interdigitation zone (IZ), corresponds to interleaved photoreceptor outer segments and RPE apical processes containing melanosomes. Fourth band components include RPE cell bodies and basal infoldings, RPE-BL, BLamD if present, contents of sub-RPE-BL space if present, and ICL-EL-OCL of BrM. RPE cell bodies contain ~1400 reflectors in two cushions of similar numerosity: lipofuscin and melanolipofuscin, with some melanosomes in the apical three-fourths, mitochondria in the basolateral three-fourths, and the middle half containing both organelle classes.[95,108] ChC-BL, ChC basal lamina; M, melanosome; ML, melanolipofuscin; Mt, mitochondria; OS, outer segments of photoreceptors.

is called the RPE-BrM complex[15] (Fig. 1). We proposed the term *RPE-BL-BrM* to incorporate the RPE-BL and basal laminar deposit (BLamD), that is, basement membrane material between the native RPE-BL and RPE plasma membrane (Fig. 1).[16–18] Between the RPE-BL and the inner collagenous layer is the sub-RPE-BL space. This potential space in young adults is filled in aged eyes with rows of lipoprotein particles in a BLinD precursor called pre-BLinD (Fig. 1) (originally, lipid wall[19]). In AMD eyes, this space contains drusen, type 1 MNV, and sequelae.[20,21] Drusen are a small fraction of the total area containing sub-RPE-BL lipid[22]; however, drusen volume is a quantifiable OCT risk indicator.[23,24] BLinD likely shares deleterious properties with drusen. Its contribution to risk has not been determined because BLinD is not visible with current OCT technology (7.0-µm axial resolution; Fig. 2). Newer technologies (2.3- to 2.8-µm resolution)[25–27] hold promise.

One aspect of AMD pathology highlighted by OCT is subretinal drusenoid deposits (SDDs; reticular pseudodrusen). First seen in 1990,[28] these extracellular deposits were localized between RPE and photoreceptors with OCT and histology in 2010.[29] They portend poor vision and risk for MNV and MA forms distinct from those of drusen.[30] BLinD/soft drusen and SDDs differ in lipid content[31,32] and are more abundant in the fovea and perifovea,[33,34] respectively, mirroring the topography of cone and rod photoreceptors.[35] Together, BLinD/soft drusen and SDD are proposed as two manifestations of one dysregulated outer retinal lipid cycling system. This system, in turn, suggests heretofore unrecognized aspects of specialized photoreceptor physiology.[33]

To fill knowledge gaps in the biology of high-risk deposits and the interpretation of OCT-based clinical imaging, we used comprehensive high-resolution histology to survey donor eyes with and without early to intermediate AMD, including one eye with in vivo imaging. We illustrated BLinD lipid content and relationship to type 1 MNV, and we quantified BLinD volume. To evaluate the hypothesis that pre-BLinD is the precursor of BLinD, we determined regional distributions, as well as SDDs in the same eyes.

Methods

Compliance

The histopathology study was approved by the institutional review board at the University of Alabama at Birmingham. Retrospective review of clinical and imaging records

Investigative Ophthalmology & Visual Science

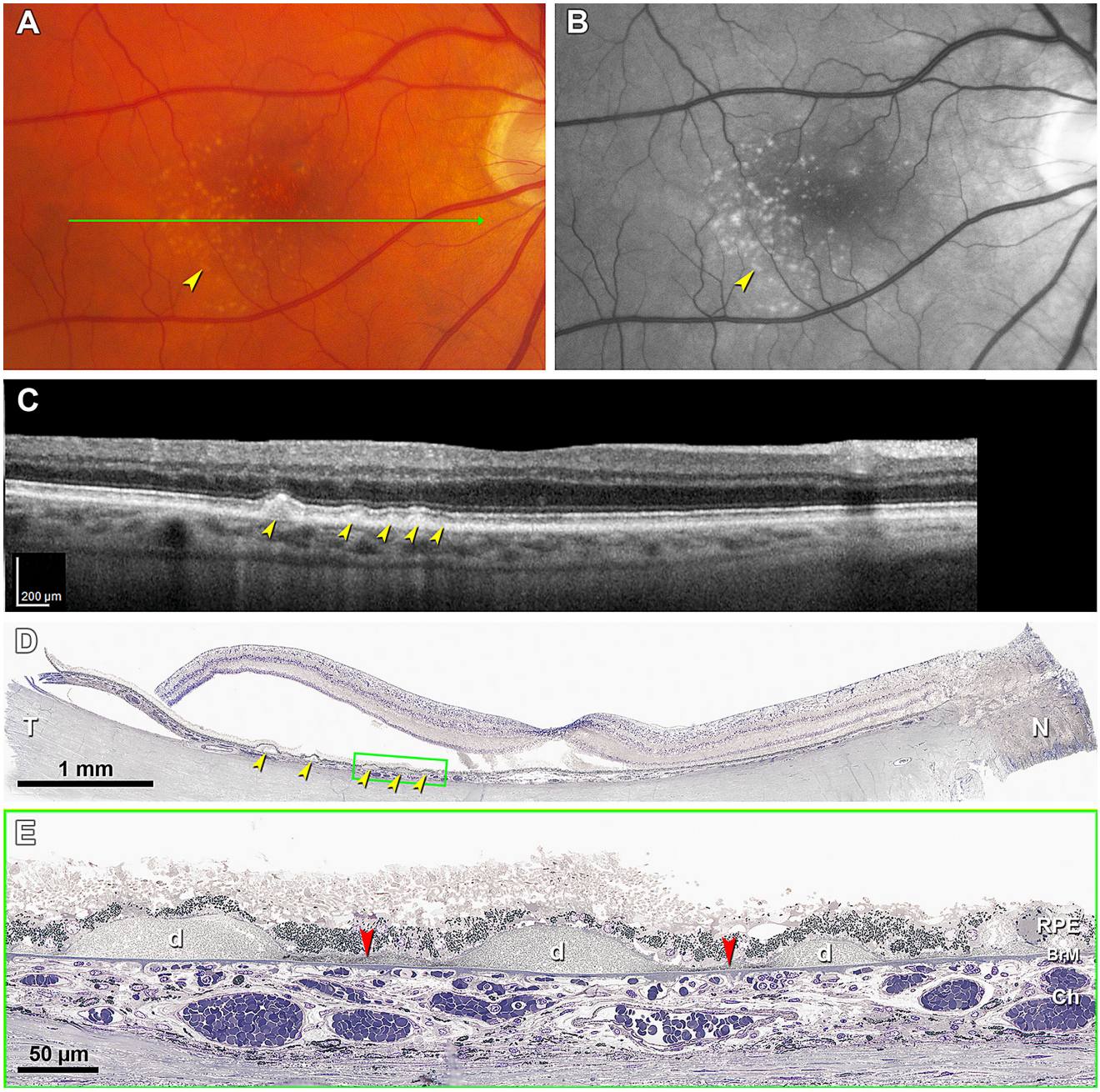

Figure 2. Soft drusen are visible in OCT-based multimodal imaging; basal linear deposit is not. (**A**) Color fundus photograph shows *yellowish* drusen (*yellow arrowhead*) in the macular region especially inferior temporal to the fovea. (**B**) Red-free image shows drusen clearly (*yellow arrowhead*). (**C**) OCT B-scan at *green arrow* in panel A shows several RPE elevations with a medium and homogeneous internal hyperreflectivity representing soft drusen (*yellow arrowheads*). (**D**) Corresponding histologic image shows soft drusen (*yellow arrowheads*) that correspond well with the B-scan. *Green* frame shows a region magnified in panel E. Retina is artifactually detached at the inner segment myoids (bacillary layer detachment). (**E**) Three soft drusen with finely granular, lightly osmophilic contents (d) are continuous with BLinD (*red arrowhead*) containing the same material. Sixty-nine-year-old white old man with early age-related macular degeneration; see Methods for details.

from one patient seen at the Department of Ophthalmology, University of California, San Francisco was approved by the institutional review boards of the University of California, San Francisco and the University of California, Berkeley. All study components complied with the Health Insurance Portability and Accountability Act of 1996 and adhered to the tenets of the Declaration of Helsinki.

Overview of Design Choices for Project MACULA

As described,[18] Project MACULA (https://projectmacula.org/) is an online digital microscope with high-resolution histology and annotated layer thicknesses of human donor eyes with and without AMD (n = 139 total, 79 used herein). Our expectation was that accurate depiction and quantification of cell and tissue features in histology could leverage

Investigative Ophthalmology & Visual Science

longitudinally tracked OCT in clinical trial image data sets and practices with long-standing OCT usage to generate a cellular-level timeline of disease.

Methods for histology were driven by the requirements of validating OCT imaging of the RPE-BL-BrM complex. Reflectivity is largely generated via Mie scattering from aqueous-lipid interfaces such as organelles. We sought subcellular resolution and comprehensive histology of tissue elements in all chorioretinal layers. We used an electron microscopy postfixation method, osmium tannic acid paraphenylenediamine,[36] and epoxy-resin submicrometer sections viewed and scanned with oil-immersion light microscopic objectives. This postfixation method stains lipids well and imparts polychromasia to toluidine blue–stained sections. Whole-slide scanning allowed seamless multiscale viewing between low magnification for context and high magnification for details, without switching objectives. Following retinal layers from less affected to more affected areas aided histologic interpretation of details in any one place.

Sampling methods were designed under the hypothesis that AMD deposits and deposit-related progression risk reflect the physiology of macular photoreceptors and supporting cells. Our prior work established accurate and unbiased counts of human photoreceptors across adulthood using computer-assisted morphometry of retinal flat mounts.[35,37] These studies showed that cones are highly concentrated in the foveal center and fall off steeply within 1 mm of eccentricity. Rods are absent in the fovea and increase to an elliptical crest of high density at 2 to 5 mm eccentricity (distance from the fovea) and extending around the optic nerve head into nasal retina.[35]

Tissue Preparation for Histology and Histologic Diagnosis

Detailed methods[38] are available in Supplementary Materials.

Assaying Layer Thicknesses and Phenotypes Within Macular Topography

At standard locations in the central and superior sections (see below), respectively, one experienced observer (C.A.C.) measured thickness of 21 layers and spaces. Simultaneously, layers were annotated with a system of cellular and laminar phenotypes using custom software with drop-down menus (ImageJ plug-in, M&A, Measurement and Annotation).[33] Locations where the sub-RPE-BL space was unevaluable due to detachment or beyond the end of the section were excluded. Detached retinas shrank more in length than the RPE-BL-BrM complex, which was anchored to sclera.[39] We corrected for this shrinkage in localizing subfoveal RPE-BL-BrM.

At each location, thickness of the sub-RPE-BL space was measured, and contents were classified as drusen, BLinD, pre-BLinD, or no lipid. Locations where contents of the sub-RPE-BL space were cellular or fibrotic, representing advanced stages of drusen, were excluded from the current analysis.[40,41] As shown in Figure 3 and Figure 4 and expanded in the Results, BLinD and pre-BLinD were grayish-pink layers that were operationally defined as undulating with nonuniform thickness or flat with uniform thickness, respectively. Detachments of the RPE-BL or BLamD from the three-layered BrM were recorded. The presence of SDDs, RPE phenotypes, BLamD thickness, and choriocapillary (ChC) ghost vessels was also recorded at the same locations. To streamline analysis, RPE phenotypes were collapsed into three categories—age-normal, dysmorphic, and atrophic—using 2015 equivalent nomenclature.[42,43]

Tissue sections were parallel to a line through the fovea and optic nerve head. The central section included the foveal rod-free zone, flanked by nasal and temporal perifovea. The superior section included superior perifovea only. Both sections were aligned on a vertical line through the foveal center. Superior sections were sampled at 0.5-mm intervals. Central sections were also sampled more densely in the fovea. Relative to the Early Treatment of Diabetic Retinopathy (ETDRS) grid,[44] locations at the foveal center plus 0.05 mm, 0.1 mm, and 0.2 mm eccentricity, nasal and temporal, fell within the central subfield. Locations at 0.4 mm, 0.6 mm, and 0.8 mm eccentricity and locations at 1.0 mm, 1.5 mm, 2.0 mm, 2.5 mm, and 3.0 mm, nasal and temporal, fell within the inner and outer rings of this grid, respectively.

BLinD Volume

For comparison with drusen volume estimates in clinical OCT scans,[23,24,45] we modeled BLinD as an object in the sub-RPE-BL space and calculated its volume using solid geometry (Supplementary Fig. S1). BLinD is thick under the fovea and thin at the macular edge.[33] BLinD was thus treated as a sum of two components, a low conical solid of rotation centered at the fovea atop a circular disk of uniform thickness. The height and slope of the cone surface were determined by fitting regression lines to the distribution of (nonzero) BLinD thicknesses as a function of eccentricity from the fovea. Locations of BLinD thickness measurements from all retinal quadrants in central and superior sections were collapsed onto one axis.[46] To reduce noise, thicknesses were determined within bins of eccentricities (0–50, 100–200, 400–600, 800–1000, 1001–1500, 1501–2000, 2001–2500, >2500 µm). From median and third quartile thicknesses for each bin, trendlines were fit, and each trendline was used to generate a conical solid of rotation. The height of the disk was determined from BLinD thickness at 3 mm eccentricity; the area of the disk was 28 mm^2. Volumes were computed for foveal-centered regions of 1 mm to 6 mm in diameter. For comparison with epidemiologic studies, we also estimated BLinD volumes within the inner and outer rings of the ETDRS grid.

Clinically Documented Case

A 69-year-old white man with human immunodeficiency virus had early AMD manifest as drusen. Color and red-free images were acquired 14 months before death. Spectral-domain optical coherence tomography (SDOCT) images were acquired 6 months before death. Eyes preserved 9 hours after death were processed as described above. Aspects of this case, including bacillary layer detachment[47] and lipid coverage of BrM,[22] have been published. In this study, we computed BLinD volume, using 22 stepped sections through the macula of the left eye (mean distance, 156 ± 17 µm; range, 90–180 µm). Thickness of each lipid category (soft drusen, BLinD, and pre-BLinD) at 500-µm intervals across each section was assessed using a custom ImageJ plug-in and used to calculate volumes.

Investigative Ophthalmology & Visual Science

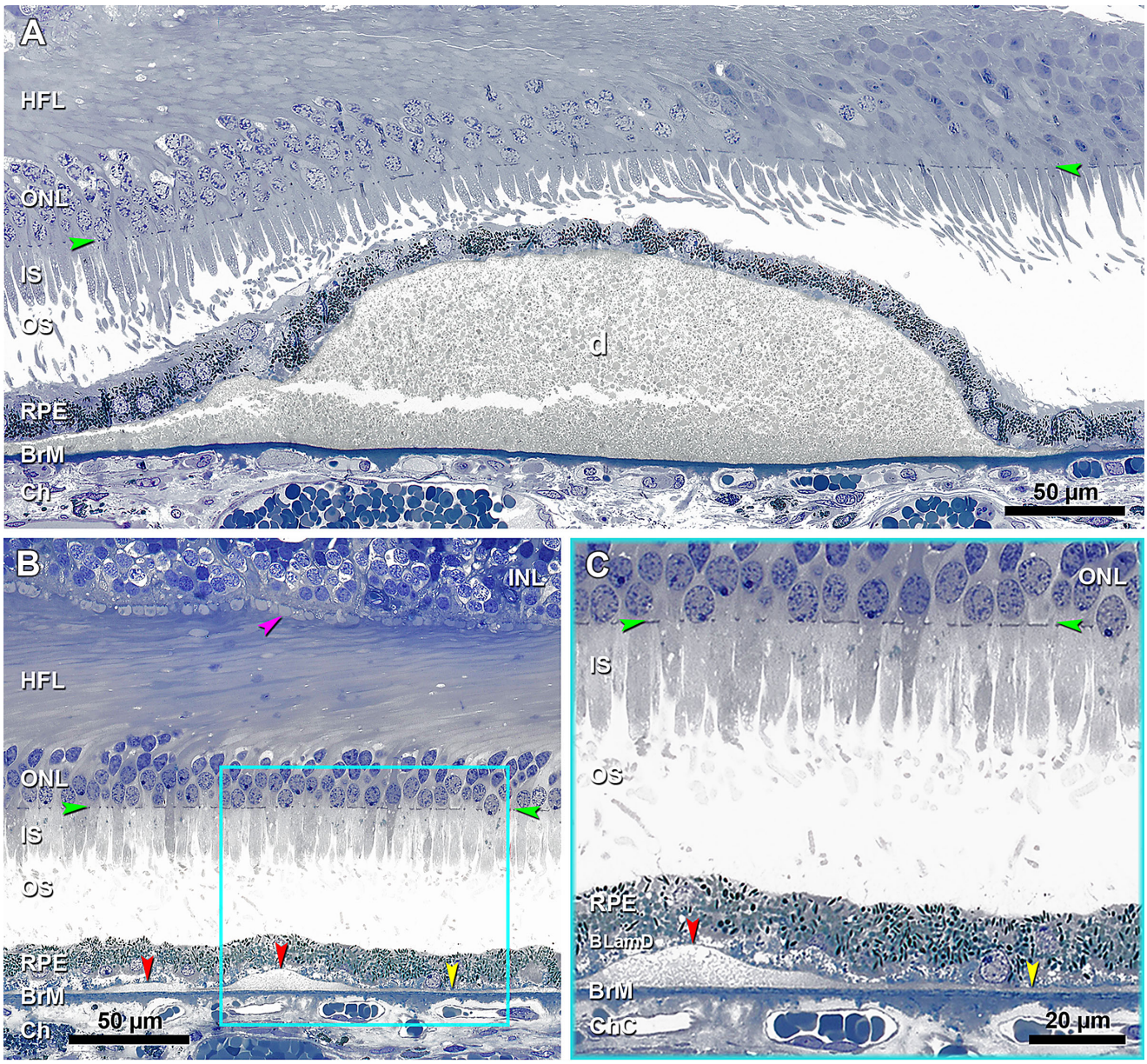

Figure 3. BLinD and soft drusen are two forms of the same deposit, and pre-BLinD is the precursor. (**A**) A large soft druse (d) is located in the sub-RPE-basal laminar space, with a granular internal structure that stains *gray* and continuous with BLinD to the *left*. The crack is artifact. Seventy-six-year-old woman. (**B**) Undulating layer of BLinD (*red arrowheads*) and flat layer of pre-BLinD (*yellow arrowhead*) are observed in the same sub-RPE-basal laminar space and have a similar internal structure and staining characteristics as soft drusen. Cone pedicles with dark staining synaptic complexes (*fuchsia arrowhead*) indicate good tissue fixation. *Teal* frame shows BLinD and pre-BLinD magnified in panel C. Artifactual retinal detachment was digitally approximated to the RPE (Photoshop). (**C**) BLinD and pre-BLinD consist of finely granular *gray*-staining material (*red and yellow arrowheads*, respectively). Pre-BLinD stains darker than BLinD. Ninety-year-old woman. Ch, choroid; HFL, Henle fiber layer; IS, inner segment; ONL, outer nuclear layer; OS, outer segment. *Green arrowheads*, external limiting membrane.

Quantitative Analysis

Data are presented as percentage of eyes affected with various features. For the regional analysis, thicknesses were pooled across eyes within diagnostic category. Drusen, BLinD, and pre-BLinD together were considered any sub-RPE-BL lipid.

Results

Twenty-five early to intermediate AMD eyes from 24 donors and 54 age-matched control eyes from 54 donors (70.8% and 53.7% female, respectively) were included in the histologic survey. Donor age was 82.4 ± 8.5 years (range, 62–97 years) and 79.7 ± 9.9 years (range, 59–94 years) in early to intermediate AMD and control groups, respectively.

Light Microscopic Appearance of BLinD, Path to Type 1 MNV

Figure 3 demonstrates histologic features of sub-RPE-BL lipid assessed in this study. Figure 3 shows BLinD continuous with both a large soft druse (Fig. 3A) and pre-BLinD

Investigative Ophthalmology & Visual Science

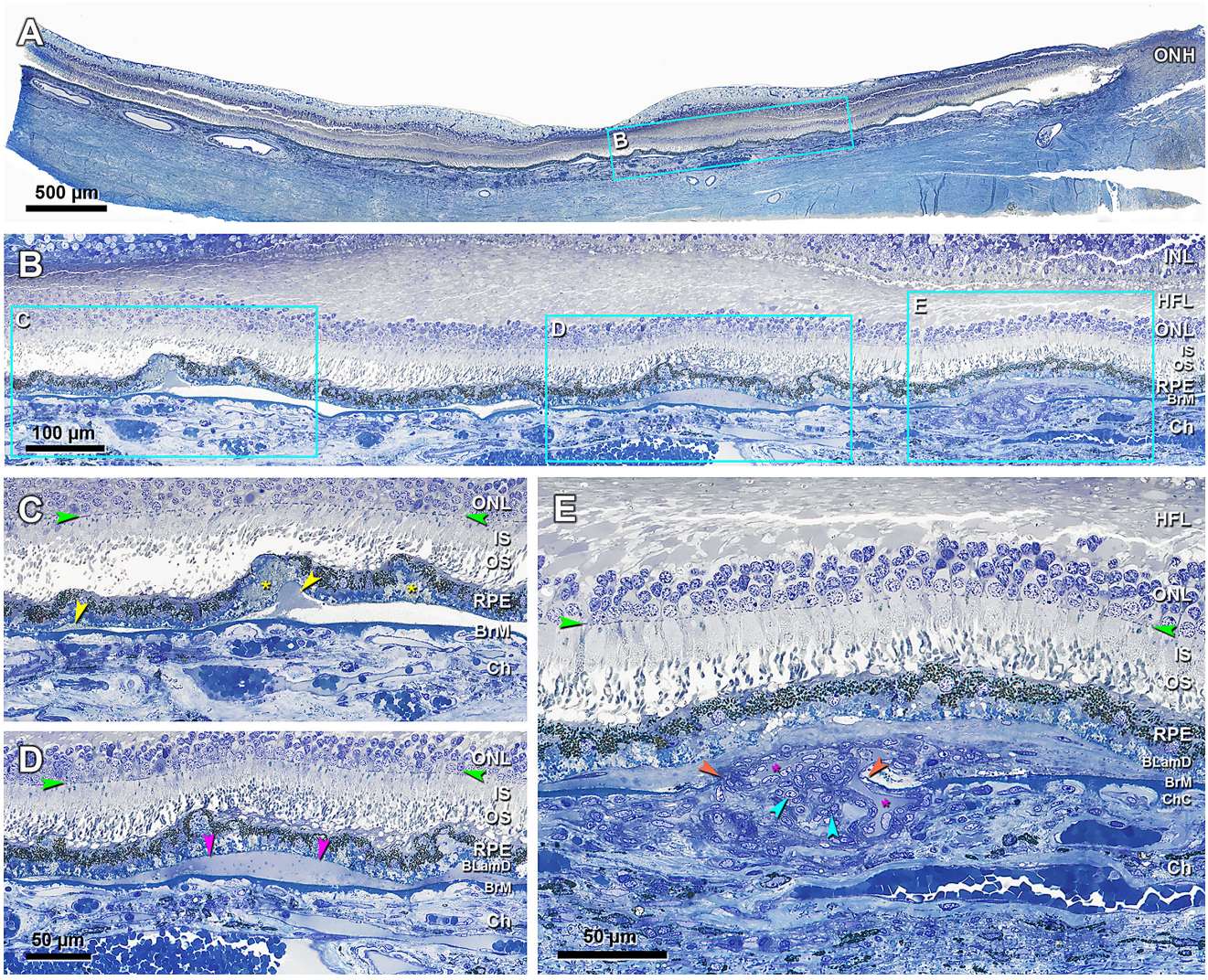

Figure 4. Continuity of basal linear deposit and soft drusen with type 1 neovascularization and exudation. (**A**) Panoramic view of a section that passes through the edge of the foveal floor of the right eye, judging from the rod-free zone and single row of ganglion cell bodies. *Teal* frame shows a region magnified in panel B. (**B**) One continuous compartment contains BLinD and soft druse (frame C), fluid (frame D), and type 1 neovascularization (frame E), magnified in panels C, D, and E, respectively. (**C**) Druse continuous with BLinD (*yellow arrowheads*) and fringe of BLinD persists at a site of artifactual separation of BLamD from the inner collagenous layer of BrM. *Yellow asterisk*, basal mound. (**D**) Fluid in the same sub-RPE-basal lamina compartment (*fuchsia arrowheads*). (**E**) Choroidal neovessels with patent lumens (*fuchsia asterisks*) pass through a break in BrM (*orange arrowheads*), accompanied by pericytes (*teal arrowheads*) and fibrous material. An 81-year-old female donor. INL, inner nuclear layer. *Green arrowheads*, ELM, external limiting membrane. *Scale bar* in D applies to C and D.

(Fig. 3B). Like soft drusen, BLinD also has a finely granular internal structure at this magnification (Fig. 3C). For optimal ultrastructural preservation, AMD eyes should be osmicated within days of primary fixation in aldehydes.[48] With archival tissue such as these, the fine structure of "membranous debris" is difficult to achieve, but differences in osmophilia (i.e., binding of osmium to nonsaturated fats) are still clear by light microscopy. BLinD is deeply stained and ragged in appearance. Pre-BLinD is more deeply stained than BLinD (Figs. 3B, C), possibly because it is more intact.

In this unbiased sample of donor eyes, it was possible to replicate a key 1997 finding by Sarks et al.[49] that type 1 MNV breached BrM and ramified under the RPE-BL in areas of "membranous debris." Panoramic high-resolution sections made it possible to demonstrate both the physical proximity of soft drusen material to type 1 MNV and its biomechanical fragility. Regarding proximity, in the sub-RPE-BL space of one continuous histologic section (Fig. 4), five elements were seen: neovascularization of choroidal origin breaching BrM, fluid, a small soft druse, BLinD fragments, and artifactual separation of BLamD from three-layered BrM at the site of BLinD. In this eye lacking a clinical history, the MNV was likely asymptomatic, judging from the small amount of fluid and the healthy-appearing outer retina. Furthermore, we reasoned that the frequency of artifactual postmortem RPE-BL detachments from the inner collagenous layer of BrM was a surrogate for biomechanical fragility of soft drusen material in vivo.[9,50,51] As shown in Table 1, many BLinD and soft drusen locations were artifactually detached in AMD eyes (25.7% and 50.6%, respectively) and less so in control eyes (14.6% and 15.6%, respectively). In both AMD and control

Table 1. Sub-RPE-BL Thickness and Detachment Rate Stratified by Sub-RPE-BL Lipid Class in AMD and Control Eyes

Characteristic	Soft Drusen	BLinD	Pre-BLinD	No Lipid
AMD eyes*				
Locations (*n*)	83	183	202	368
Thickness (μm)	40.3 (16.1, 119.0)	1.8 (1.2, 3.8)	0.8 (0.6, 1.1)	0
Detachment rate (*n*/%)	42/50.6	47/25.7	1/0.5	2/0.5
Control eyes†				
Locations (*n*)	32	96	405	1183
Thickness (μm)	7.7 (4.8, 15.2)	1.4 (1.0, 2.2)	0.8 (0.5, 1.1)	0
Detachment rate (*n*/%)	5/15.6	14/14.6	4/1.0	2/0.2

Data are number of locations (*n*), thickness (μm), and percentage (%).

* Twenty-seven locations in AMD eyes were excluded because they were nonevaluable, and 11 locations were excluded due to cellular contents or scar.

† Fifty-eight locations in control eyes were excluded because they were nonevaluable, and 7 locations were excluded due to cellular contents or fluid.

Table 2. RPE Phenotypes Stratified by Sub-RPE-BL Lipid Class in AMD and Control Eyes

Characteristic	Age-Normal RPE	Dysmorphic RPE	Atrophic RPE
AMD ($n = 836$), *n*/%			
No lipid	199/54.1	162/44.0	7/1.9
Pre-BLinD	66/32.7	135/66.8	1/0.5
BLinD/drusen	70/26.3	188/70.7	8/3.0
Control ($n = 1716$), *n*/%			
No lipid	1082/91.5	101/8.5	0/0.0
Pre-BLinD	316/78.0	89/22.0	0/0.0
BLinD/drusen	79/61.7	48/37.5	1/0.8

Data are present as number and percentage (%) of RPE phenotypes as defined in the Methods in each sub-RPE-BL lipid category.

Age-normal RPE included uniform and nonuniform. Dysmorphic RPE included very nonuniform, dissociated, shedding, intraretinal, entombed, sloughed, bilaminar, and vacuolated. RPE was atrophic with and without BLamD.

eyes, detachments were rarely observed in locations with pre-BLinD or lacking sub-RPE-BL lipid. No detachments of BLamD from the basal RPE were seen.

Biometrics: Thicknesses, Volume, Associations, and Topography

To compare thicknesses of lipid in the sub-RPE-BL space (BLinD/drusen, pre-BLinD, or no Sub-RPE-BL lipid) in AMD and control eyes, a total of 836 locations from the early to intermediate AMD eyes and 1716 locations from the control eyes were evaluated (Table 1). Thicknesses in many of the AMD eyes were published previously[52]; thicknesses from control eyes are herein reported for the first time. Median BLinD thickness in AMD and control eyes was 1.8 μm and 1.4 μm, respectively. Median thickness of pre-BLinD was 0.8 μm in both.

To evaluate the association of sub-RPE-BL lipid with pathology in adjoining tissue layers, RPE phenotypes, BLamD thickness, and the presence of ChC ghosts were stratified by lipid class in early to intermediate AMD and control eyes (Tables 2, 3, and 4, respectively). In both AMD and control eyes, the distribution of RPE cell morphologies shifted toward abnormal with worse sub-RPE-BL lipid. In AMD eyes, median BLamD thickness was 1.9 μm, 3.2 μm, and 4.1 μm for locations with no sub-RPE-BL lipid, pre-BLinD, and BLinD/drusen, respectively. In control eyes, median BLamD thickness was zero in locations with no sub-RPE-BL lipid and pre-BLinD and 1.8 μm in locations with BLinD/drusen. The percentage of ChC ghosts increased with sub-RPE-BL lipid classes in both AMD (7.6%, 14.9%, and 19.2% for no sub-RPE-BL lipid, pre-BLinD, and BLinD/drusen, respectively) and control (3.0%, 8.1%, and 13.3%) eyes.

We estimated BLinD volume under several assumptions, a geometric model (Supplementary Fig. S1), and 183 measured thicknesses. Figure 5 shows BLinD thickness as a function of eccentricity from the foveal center and regression lines used to estimate BLinD volume in fovea-centered regions of different diameter (Table 5). To compare with drusen volume measured in longitudinal OCT studies, we estimated BLinD volume within a 3-mm diameter circle as 0.0153 mm^3 and 0.0315 mm^3 for the median and third quartile regression lines, respectively (Table 5). In a clinically documented early

Table 3. BLamD Thickness Stratified by Sub-RPE-BL Lipid Class

Characteristic	AMD ($n = 836$)	Control ($n = 1716$)
No lipid (μm)	1.9 (0, 6.4)	0 (0, 0)
Pre-BLinD (μm)	3.2 (1.3, 9.1)	0 (0, 2.3)
BLinD/drusen (μm)	4.1 (1.2, 8.0)	1.8 (0, 4.4)

Data are presented as mean ± SD.

Table 4. Choriocapillaris Ghosts Stratified by Sub-RPE-BL Lipid Class

Characteristic	AMD ($n = 836$)	Control ($n = 1716$)
No lipid (*n*/%)	28/7.6	35/3.0
Pre-BLinD (*n*/%)	30/14.9	33/8.1
BLinD/drusen (*n*/%)	51/19.2	17/13.3

Data are present as number and percentage (%) of choriocapillaris ghosts in each sub-RPE-BL lipid category.

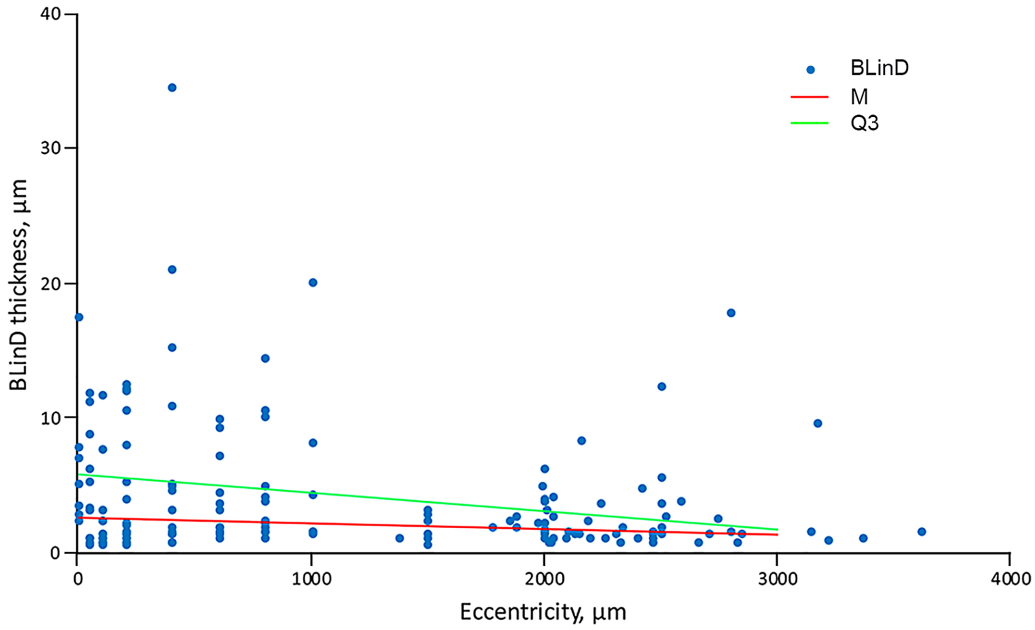

Figure 5. Basal linear deposit thickness in age-related macular degeneration eyes. The horizontal axis represents eccentricity, that is, distance from the foveal center (zero point). The vertical axis represents the thickness of BLinD. *Blue dots* represent BLinD thickness assessed at 168 different locations, as described in the Methods. Data from all retinal quadrants are collapsed onto one axis. Eccentricities were collapsed into bins as described in the Methods and the median (M) and third quartile thickness value (Q3) in each bin calculated. Two trendlines were created (M, *red line*; Q3, *green line*) and used to estimate volumes of BLinD shown in Table 2.

Table 5. Volume of Basal Linear Deposit in Concentric Macular Regions

Region	Volume, Median (mm^3)	Weighted, Median (mm)	Volume, Quartile 3 (mm^3)	Weighted, Quartile 3 (mm)
r (0.5 mm)	0.0019	0.0024	0.0042	0.0054
r (1.5 mm)	0.0153	0.0022	0.0315	0.0045
r (2.5 mm)	0.0373	0.0019	0.0692	0.0035
r (3.0 mm)	0.0499	0.0018	0.0864	0.0031
Inner ring	0.0134	0.0021	0.0273	0.0043
Outer ring	0.0346	0.0016	0.0549	0.0026

Regions are centered on the fovea. The volume of BLinD was calculated based on the geometric model of BLinD distribution in the Supplementary Figure S1. Which has also been weighted by region area. r = 0.5, r = 1.5, and r = 3.0 correspond to the outer boundary of the central subfield, inner ring, and outer ring of Early Treatment of Diabetic Retinopathy Study grading grid for color fundus photography.[44]

r, radius.

AMD eye (Fig. 2), BLinD volume within a 3-mm diameter circle was calculated as 0.018 mm^3.

Figure 6 shows sub-RPE-BL lipid accumulation in macular subregions in AMD and control eyes (836 and 1716 locations, respectively). Three observations can be made. First, compared with control eyes, more or a similar number of locations in AMD eyes had any sub-RPE-BL lipid. AMD eyes exceeded control eyes by factors of 1.14, 1.27, 2.45, and 0.99 in foveal, nasal, superior and temporal regions, respectively. Second, the percentage of locations in AMD eyes and in control eyes with either BLinD/drusen (43.9% AMD and 13.9% control) or pre-BLinD (15.4% AMD and 37.9% control) was highest in the fovea. Accordingly, the percentage of locations without any sub-RPE-BL lipid was lowest in the fovea in both groups. Third, in all regions, and especially the fovea, BLinD/drusen was more prominent than pre-BLinD (43.9% vs. 15.4%) in AMD eyes, whereas in control eyes, BLinD/drusen was more prominent than pre-BLinD (13.9% vs. 37.9%).

Comparison of BLinD and SDDs

BLinD and SDDs have been linked due to their differences in lipid composition and complementary topographic distributions resembling the photoreceptors. Figure 7 compares the lipid content of BLinD, SDDs, and lipid globules,[53,54] the latter serving as a positive control for osmophilia. Here, SDD appears lightly stained (Fig. 7), distinct from BLinD and consistent with published electron micrographs[55] showing a solid material with regularly spaced membranous inclusions.

We also compared the percentage of locations with SDDs to those with BLinD/drusen in AMD eyes and control eyes (Fig. 8). In contrast to sub-RPE-BL lipid (Fig. 7), the percentage of locations with SDDs was low (but not zero) in the fovea in both AMD and control eyes and highest in the superior perifovea in AMD eyes and the nasal perifovea in control eyes. The percentage of locations with SDDs in AMD eyes was higher than in control eyes by factors of 5.2, 2.5, 6.0, and 24.7 in the fovea, nasal, superior, and temporal subregions,

Investigative Ophthalmology & Visual Science

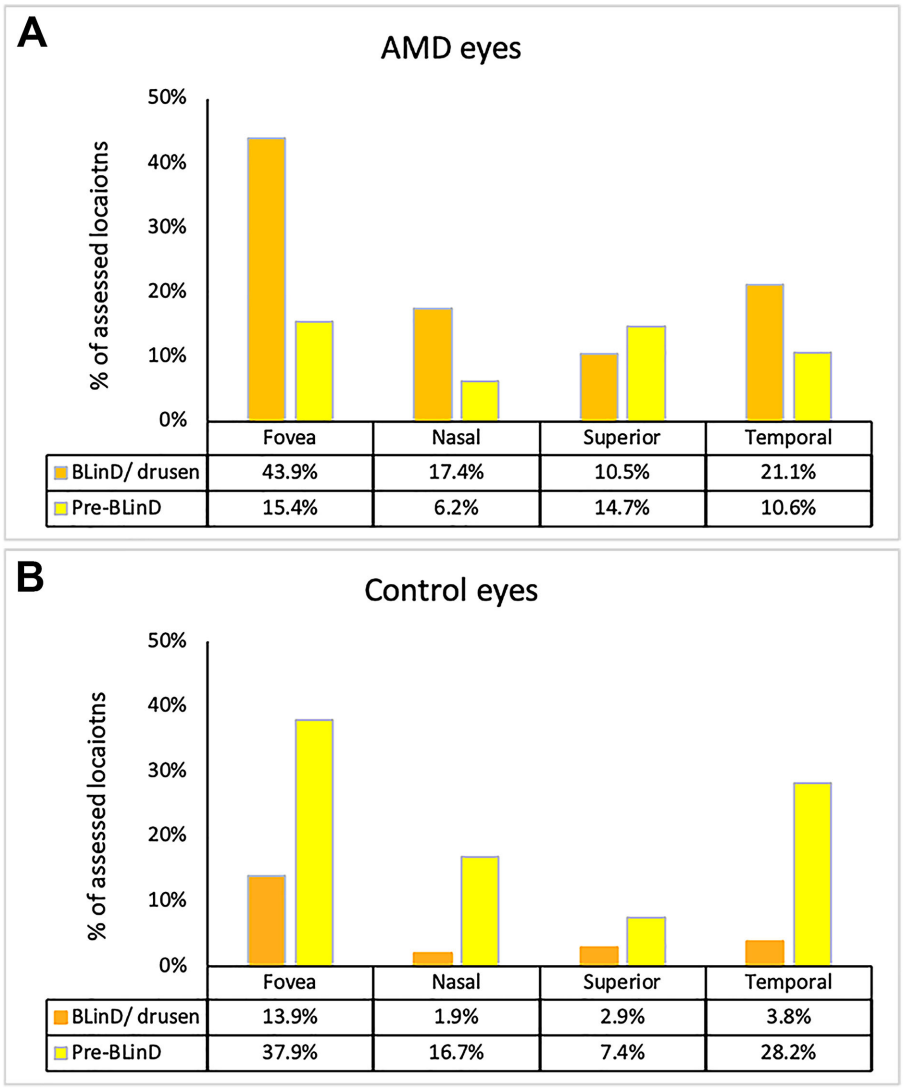

Figure 6. Sub-RPE-BL lipid accumulation is topographically organized in aged and age-related macular degeneration fundus. One foveal and three perifoveal fundus regions were defined in central and superior sections, as described in the Methods. (**A**) Percentage of 836 locations with BLinD/drusen and pre-BLinD in different regions in 25 AMD eyes. (**B**) Percentage of 1716 locations with BLinD/drusen or pre-BLinD in different fundus regions in 54 control eyes. In AMD eyes and control eyes, the percentage of locations with BLinD/drusen or pre-BLinD is highest in the fovea. The percentage of locations with any sub-RPE-BL lipid in AMD eyes is 1.14 times, 1.27 times, 2.45 times, and 0.99 times that of the control eyes in fovea, nasal, superior, and temporal regions, respectively. In the fovea, AMD and control eyes have a similar total number of locations with sub-RPE-BL lipid, with proportionally more BLinD and less pre-BLinD in AMD eyes.

respectively (i.e., much greater than the excess of sub-RPE-BL lipid in AMD eyes over control eyes).

Discussion

Taken with our recent reports on BLamD and SDDs,[18,56] this report advances a comprehensive description of AMD pathology to support multimodal OCT-based clinical imaging and a multilayer progression timeline. Soft drusen are the earliest discovered and largest risk factor for progression to end stages. Despite extraordinary epidemiologic evidence for causality,[2] drusen are just one of many actors in extant theories of AMD pathophysiology. One reason is that human eye studies require systematic tissue collection to capture all AMD stages and specialized techniques to differentiate soft drusen material from RPE-BL above and ICL below,[18] challenges we herein address.

With high-resolution histology and color photodocumentation, we affirmed that BLinD and soft drusen constitute one oil spill in the sub-RPE-BL space leading to type 1 MNV, the most common type, and exudation.[21] Our recent clinicopathologic correlations also clearly showed type 1 MNV and soft drusen material confined to this compartment.[41,57] The laminar location of type 1 MNV may be difficult to discern in low-magnification views of paraffin histology.[51] Nevertheless, in the Sub-Macular Surgery Trial, little BLinD or soft drusen was found in excised specimens with MNV.[58] This absence suggested that BLinD was never present, that it was lost in processing, or that MNV grew into space previously occupied by BLinD to replace or remove the deposit.[59] Since the clinical manifestations of abundant BLinD were known to be soft drusen and risk factors for MNV, the latter interpretation was deemed more likely,[59] as supported by our histology. A high proportion (81%) of newly presenting

Investigative Ophthalmology & Visual Science

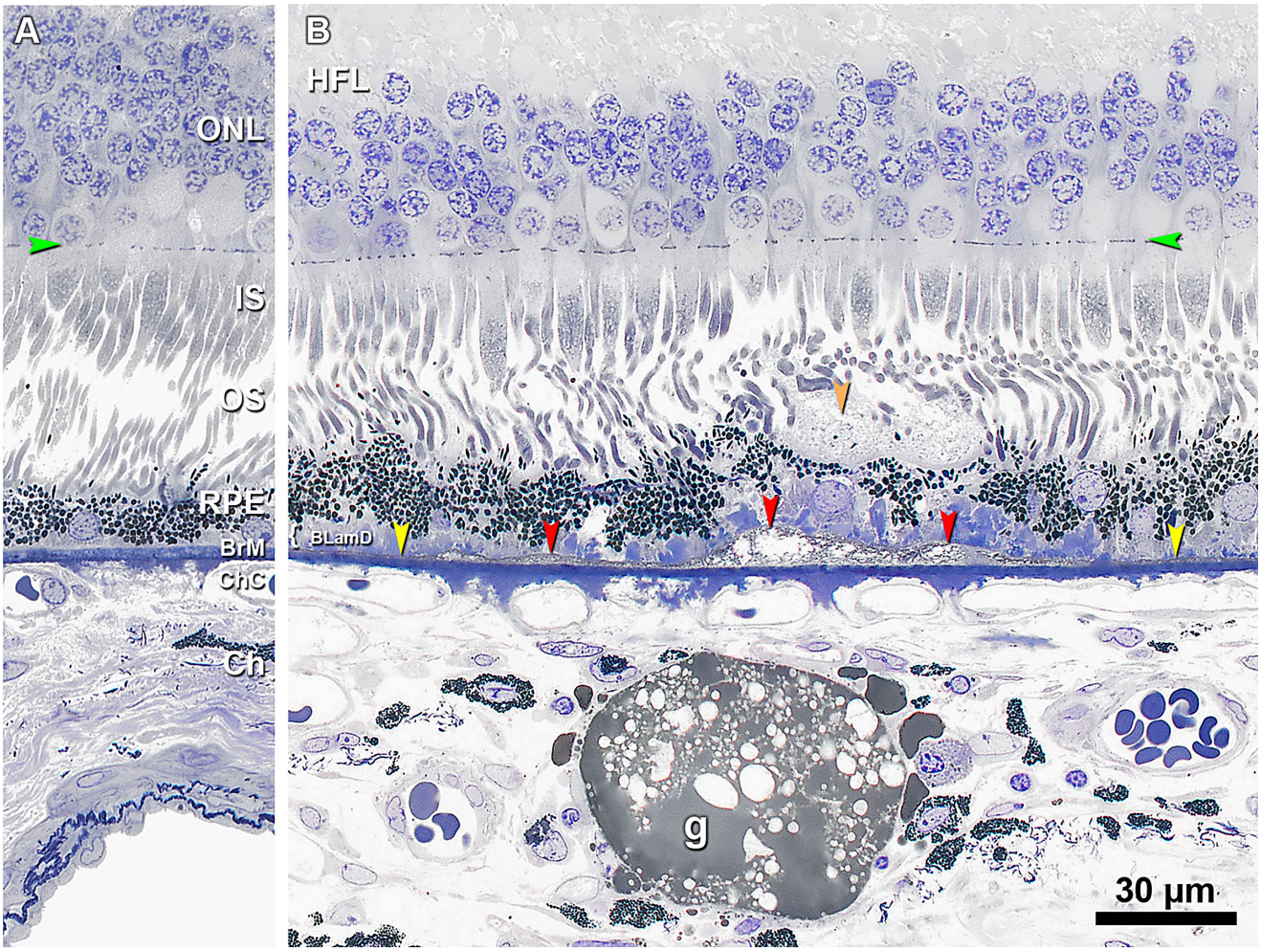

Figure 7. Subretinal drusenoid deposit is less lipid rich than basal linear deposit. (**A**) The sub-RPE-BL space is normally devoid of lipid. (**B**) 60 µm away from panel A. BLinD (*red arrowheads*) is continuous with and thicker than pre-BLinD (*yellow arrowheads*) in the sub-RPE-BL space. BLinD is operationally distinguished from pre-BLinD by its undulating profile. SDD (*orange arrowhead*) is observed on top of wavy RPE, with a finely granular texture, several RPE melanosomes, and minimal osmophilia relative to BLinD. A choroidal lipid globule (g) is *deep gray* and serves as a positive control for osmophilic lipids.[53] Eighty-seven-year-old man. *Green arrowheads*, external limiting membrane. *Scale bar* in B applies to A and B.

MNV is subfoveal, whether identified angiographically[60] or on OCT,[61] and MNV tends to enlarge toward the fovea.[62] We suggest that soft drusen material is a source of peroxidizable lipids that are proinflammatory and biomechanically fragile, thus providing a low-resistance matrix. Invading vessels thus may enter a cleavage plane that insidiously widens toward the fovea due to thick BLinD. Vascular endothelium may also proliferate toward high VEGF levels[63] at foveal RPE, which is elevated from ChC (Table 5; also Sura et al.[18]).

By showing that pre-BLinD appears in the same macular regions as BLinD/drusen, we solidified pre-BLinD as a drusen precursor. Furthermore, AMD and control eyes had similar frequency of foveal locations with any sub-RPE-BL lipid, with proportionally more BLinD and less pre-BLinD in AMD eyes (Fig. 6). The role in drusen formation of ChC dysfunction is highlighted by the numerous ChC ghosts in locations with advanced sub-RPE-BL lipid (Table 4).[64] Data are interpretable within a well-supported model of an atherosclerosis-like AMD progression that is vascular originated and lipoprotein propelled.[13] This model posits a lifelong release by RPE to the circulation of unneeded lipids in large lipoproteins. Neurosensory retina and RPE are relatively functional throughout adulthood. BrM/ChC fails slowly, leading to the accumulation of materials that reflect normal physiology but become modified and toxic over time. Lipids are sequestered first in BrM, then the sub-RPE-BL space, and then within BLamD as basal mounds.[18] The impact on photoreceptors of increased pathlength to the circulation is virtual ischemia, affecting nutrition (see below) and possibly oxygen levels.

Drusen are only the visible part of an oil spill, and for the first time, we estimated the volume of invisible BLinD. We previously showed in this clinically documented case that drusen occupied 14% of the total area with sub-RPE-BL lipid, compared to 46% occupied by BLinD.[22] Drusen volume on OCT entails measuring the distance between the elevated RPE layer and BrM[65–67] and currently omits BLinD and elevations <19 µm in height. Patients with volume >0.03 mm^3 have a 1.4- to 4-fold higher risk for developing advanced AMD compared with lesser drusen volumes.[23,24] Volume >0.03 mm^3 within a 3-mm diameter circle was proposed as an endpoint for clinical trials[45,68] and one part of a

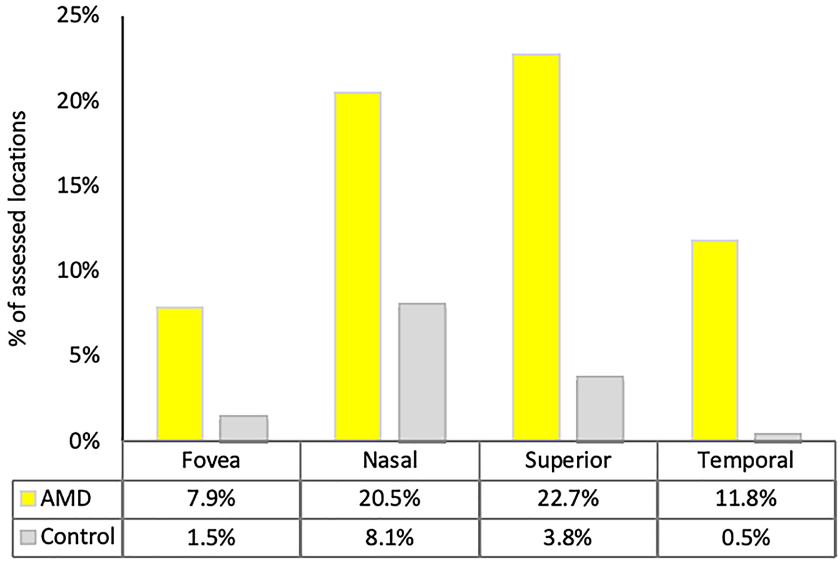

Figure 8. Subretinal drusenoid deposit is topographically organized in aged and in age-related macular degeneration fundus. *Yellow* columns indicate percentage of 836 locations with SDDs in different macular subregions in 25 AMD eyes. *Gray* columns indicate percentage of 1716 locations with SDDs in different macular subregions in 54 control eyes. The percentage of locations with SDDs was lower in the fovea than in the other subregions in both groups. The percentage of locations with SDDs in AMD eyes is higher than in control eyes by factors of 5.2, 2.5, 6.0, and 24.7 in the fovea, nasal, superior, and temporal subregions, respectively. Percentages are overall lower than those for sub-RPE-BL lipid in Figure 6 (note different scaling on Y-axis).

composite progression risk indicator[24,69] that can be estimated qualitatively with speed and reliability.[70] Depending on assumption, our calculated volume for BLinD (0.0315 mm^3) could reach this clinical criterion and imperceptibly push individual patients into a danger zone of high progression risk.

The preferential subfoveal accumulation of soft drusen material in this study and our published analysis of BLamD[38] is consistent with a hypothesis that a major source of the unneeded lipids deposited in drusen is plasma high-density lipoprotein (HDL) delivering the xanthophyll carotenoid pigments lutein and zeaxanthin.[71] HDL is taken up at receptors by RPE[72] for transfer of carotenoids to foveal Müller glia and cones.[73] This idea received support from a recent study[74] showing that a sharp peak of foveal drusen volume in OCT matches the distribution of drusen-related progression risk and xanthophyll pigment assessed with two-wavelength autofluorescence imaging. Furthermore, functional impact of BLinD and drusen on vision is suggested by the topography of rod-mediated dark adaptation (RMDA), a dynamic measure of retinoid resupply to the photoreceptors from the circulation. Delayed RMDA is a functional biomarker for AMD onset.[75] A recent study[76] agnostically revealed via deep learning that structural OCT features predictive for delayed RMDA fall within a circular foveal-centered oil spill, defined by epidemiology,[3] clinical imaging,[74] and the current histology. This entire sequence plausibly unfolds under the lifetime systemic and intraocular influence of HDL genes[77,78] (*APOE, CETP, LIPC, ABCA1*), the second largest pathway implicated by AMD genetics after complement.

We showed for the first time that SDDs in older normal eyes have low foveal and high perifoveal predilection, as they do in AMD eyes, in both histology and clinical imaging.[34,79] High SDD frequency in AMD eyes relative to control eyes (Fig. 8) should be interpreted cautiously, because detachment of the retina from RPE is common in postmortem specimens (73% of locations in the AMD eyes).[33] Assuming similar detachment rates in control eyes, it is possible that small SDDs may have been lost to detection. Nevertheless, topographic analysis uses whole sections subject to the same artifacts. Notably, this analysis revealed that foveal SDD prevalence is not zero, so the overall picture of SDDs tracking rod photoreceptors must also include other factors. Furthermore, SDD distribution does not translate into a topographical relationship of SDDs with intraretinal MNV,[80,81] which occurs predominantly in the ETDRS temporal inner ring.[80]

The current study demonstrated that relative to BLinD/drusen, SDDs have a lesser concentration of osmophilic lipid. Data thus support previous findings of unesterified cholesterol in both SDDs and drusen and esterified cholesterol in drusen only[31,32,82] (see also Figures 7 and 9 in Chen et al.[56]). Although some drusen proteins appear in SDDs,[32,83] our new data along with previously reported CD59 immunoreactivity,[84] lack of mineralization,[85] association with non-AMD retinopathies, differential risk for MNV subtypes, and poor response to laser prophylaxis collectively demonstrate that SDD biology differs importantly from that of drusen.[56,86] Theories for SDD formation propose dysregulation of previously unappreciated outer retinal lipid cycling mechanisms involving lipoprotein particles containing apolipoprotein E and interphotoreceptor retinoid binding protein.[30,33] An urgent need for future research is an ultrastructural description of earliest SDDs.

Our data can support existing, prototype, and experimental technologies to image BLinD in vivo.[87–89] Because soft drusen are hypofluorescent in indocyanine green angiography,[90] a widespread late-phase hypofluorescence across aged macula was suggested to reveal BLinD.[87,91] Advanced OCT technologies have adequate resolution to separate sublayers within the RPE-BL-BrM complex.[25,27,92] Deconvolution of multispectral tissue autofluorescence signals

indicates a distinct emission spectrum for drusen and BLinD that could be exploited in a clinical imaging device.[89]

Strengths of this study include unbiased and systematic review of many donor eyes at short death-to-preservation interval; one eye with in vivo multimodal imaging; comprehensive, high-resolution, lipid-preserving histology and photodocumentation on all eyes; a first estimate of BLinD volume; and first demonstrations of BLinD and SDD topography in normal aged eyes. The use of digital sections scaled to micrometers, a fovea-centered coordinate system, and systematic sampling enabled comparisons of morphological data across eyes and referenced to epidemiology. Limitations are the use of only two sections from each eye, lack of electron microscopy for deposit ultrastructure, and underrepresentation of eyes with large drusen in the Project MACULA sample due to their use in prior studies.[93]

By comparing AMD cases to controls with appropriate tissue, microscopy, and analysis techniques, we find that BLinD/soft drusen culminate years of subfoveal lipid accumulation. In contrast, SDDs are detected relatively late in life, mostly extra-foveally, and with currently unknown precursors. Our data underscore the need for imaging technology and analysis tools with high spatial resolution and precision in three dimensions for both deposits. Of therapeutic relevance, our data support drusen reduction and/or detoxification, deposit management for replacement cell approaches, and improved transport from the circulation as an objective. Research priorities are comprehensive compositional[94] and ultrastructural[95] studies of deposits and model systems that replicate or probe aspects of lipid transfer among outer retinal cells and ChC.[85,96–99]

According to R.F. Spaide[86] AMD is a deposit-driven disease in which both SDDs and drusen can lead to MA and MNV. Here we focused on a transition to MNV; a transition to MA is described elsewhere.[40,100–102] We extend this proposal by showing that drusen and SDD topographies reflect those of cone and rod photoreceptors in control eyes as well as AMD. Linking progression to molecular pathways that sustain cones and rods also links AMD to the evolutionary biology of vision, a radically simplifying idea.

Acknowledgments

The authors thank Advancing Sight Network (formerly Alabama Eye Bank, Birmingham, AL, USA) and Gerry Estrella Jr., MD, CTBS, CEBT (tissue recovery manager—Bay/Northern Region, California Transplant Donor Network, San Leandro, CA, USA), for timely retrieval of donor eyes.

Supported by The Macula Foundation, New York; an anonymous donor to University of Alabama at Birmingham; and Heidelberg Engineering. The Project MACULA website and the recovery of human donor eyes for research has been supported by National Institutes of Health grant R01EY06019, EyeSight Foundation of Alabama, International Retinal Research Foundation, the Edward N. and Della L. Thome Foundation, the Arnold and Mabel Beckman Initiative for Macular Research, and institutional support from Research to Prevent Blindness. The recovery of the clinically documented case was made possible by the Foundation Fighting Blindness. Purchase of the slide scanner was made possible by the Carl G. and Pauline Buck Trust.

Disclosure: **L. Chen**, None; **J.D. Messinger**, None; **D. Kar**, None; **J.L. Duncan**, (C) Sparing Vision, Vedere Bio, Astellas, DTx Pharma, Editas Inc, Eloxx, ProQR Therapeutics, Eyevensys, Gyroscope Therapeutics, Ionis, AGTC, Spark Therapeutics (F) Biogen/Nightstarx Therapeutics (I) RxSight (spouse); **C.A. Curcio**, Heidelberg Engineering and Genentech/Roche (F); MacRegen Inc (I, I for spouse)

References

1. Flaxman SR, Bourne RRA, Resnikoff S, et al. Global causes of blindness and distance vision impairment 1990–2020: a systematic review and meta-analysis. *Lancet Glob Health*. 2017;5:e1221–e1234.
2. Klein R, Klein BE, Knudtson MD, Meuer SM, Swift M, Gangnon RE. Fifteen-year cumulative incidence of age-related macular degeneration: the Beaver Dam Eye Study. *Ophthalmology*. 2007;114:253–262.
3. Wang JJ, Rochtchina E, Lee AJ, et al. Ten-year incidence and progression of age-related maculopathy: the Blue Mountains Eye Study. *Ophthalmology*. 2007;114:92–98.
4. Ferris FL, III, Wilkinson CP, Bird A, et al. Clinical classification of age-related macular degeneration. *Ophthalmology*. 2013;120:844–851.
5. Guymer RH, Baird PN, Varsamidis M, et al. Proof of concept, randomized, placebo-controlled study of the effect of simvastatin on the course of age-related macular degeneration. *PLoS One*. 2013;8:e83759.
6. Vavvas DG, Daniels AB, Kapsala ZG, et al. Regression of some high-risk features of age-related macular degeneration (AMD) in patients receiving intensive statin treatment. *EBioMedicine*. 2016;5:198–203.
7. Rudolf M, Mir Mohi Sefat A, Miura Y, et al. ApoA-I mimetic peptide 4F reduces age-related lipid deposition in murine bruch's membrane and causes its structural remodeling. *Curr Eye Res*. 2018;43:135–146.
8. Rudolf M, Curcio CA, Schlötzer-Schrehardt U, et al. Apolipoprotein A-I mimetic peptide L-4F removes Bruch's membrane lipids in aged non-human primates. *Invest Ophthalmol Vis Sci*. 2019;60:461–472.
9. Sarks SH, van Driel D, Maxwell L, Killingsworth M. Softening of drusen and subretinal neovascularization. *Trans Ophthalmol Soc U K*. 1980;100:414–422.
10. Curcio CA, Johnson M, Huang J-D, Rudolf M. Aging, age-related macular degeneration, and the response-to-retention of apolipoprotein B-containing lipoproteins. *Prog Ret Eye Res*. 2009;28:393–422.
11. Sarks JP, Sarks SH, Killingsworth MC. Evolution of geographic atrophy of the retinal pigment epithelium. *Eye*. 1988;2:552–577.
12. Curcio CA, Johnson M, Huang J-D, Rudolf M. Apolipoprotein B–containing lipoproteins in retinal aging and age-related maculopathy. *J Lipid Res*. 2010;51:451–467.
13. Curcio CA. Soft drusen in age-related macular degeneration: biology and targeting, via the oil spill strategy. *Invest Ophthalmol Vis Sci*. 2018;59:AMD160–AMD181.
14. Curcio CA. Antecedents of soft drusen, the specific deposit of age-related macular degeneration, in the biology of human macula. *Invest Ophthalmol Vis Sci*. 2018;59:AMD182–AMD194.
15. Staurenghi G, Sadda S, Chakravarthy U, Spaide RF. Proposed lexicon for anatomic landmarks in normal posterior segment spectral-domain optical coherence tomography: the IN*OCT Consensus. *Ophthalmology*. 2014;121:1572–1578.
16. Gass JDM. *Stereoscopic Atlas of Macular Diseases: Diagnosis and Treatment*. 4th ed. St Louis, MO: Mosby; 1997.
17. Bressler SB, Bressler NM, Sarks SH, Sarks JP. Age-related macular degeneration: nonneovascular early AMD, intermediate AMD, and geographic atrophy. In: Ryan SJ, ed. *Retina*. St Louis, MO: Mosby; 2006:1041–1074.

Investigative Ophthalmology & Visual Science

18. Sura AA, Chen L, Messinger JD, et al. Measuring the contributions of basal laminar deposit and Bruch's membrane in age-related macular degeneration. *Invest Ophthalmol Vis Sci*. 2020;61:19.
19. Ruberti JW, Curcio CA, Millican CL, Menco BP, Huang JD, Johnson M. Quick-freeze/deep-etch visualization of age-related lipid accumulation in Bruch's membrane. *Invest Ophthalmol Vis Sci*. 2003;44:1753–1759.
20. Killingsworth MC. Angiogenesis in early choroidal neovascularization secondary to age-related macular degeneration. *Graefes Arch Clin Exp Ophthalmol*. 1995;233:313–323.
21. Sarks JP, Sarks SH, Killingsworth MC. Morphology of early choroidal neovascularization in age-related macular degeneration: correlation with activity. *Eye*. 1997;11:515–522.
22. Chen L, Messinger JD, Sloan KR, et al. Abundance and multimodal visibility of soft drusen in early age-related macular degeneration: a clinicopathologic correlation. *Retina*. 2020;40:1644–1648.
23. Abdelfattah NS, Zhang H, Boyer DS, et al. Drusen volume as a predictor of disease progression in patients with late age-related macular degeneration in the fellow eye. *Invest Ophthalmol Vis Sci*. 2016;57:1839–1846.
24. Nassisi M, Lei J, Abdelfattah NS, et al. OCT risk factors for development of late age-related macular degeneration in the fellow eyes of patients enrolled in the HARBOR study. *Ophthalmology*. 2019;126:1667–1674.
25. Zhang T, Kho AM, Srinivasan VJ. Improving visible light OCT of the human retina with rapid spectral shaping and axial tracking. *Biomed Opt Express*. 2019;10:2918–2931.
26. Lee B, Chen S, Moult EM, et al. High-speed, ultrahigh-resolution spectral-domain OCT with extended imaging range using reference arm length matching. *Trans Vis Sci Tech*. 2020;9:12.
27. Shirazi MF, Brunner E, Laslandes M, Pollreisz A, Hitzenberger CK, Pircher M. Visualizing human photoreceptor and retinal pigment epithelium cell mosaics in a single volume scan over an extended field of view with adaptive optics optical coherence tomography. *Biomed Opt Express*. 2020;11:4520–4535.
28. Mimoun G, Soubrane G, Coscas G. Macular drusen [in French]. *J Fr Ophtalmol*. 1990;13:511–530.
29. Zweifel SA, Spaide RF, Curcio CA, Malek G, Imamura Y. Reticular pseudodrusen are subretinal drusenoid deposits. *Ophthalmology*. 2010;117:303–312.e.301.
30. Spaide RF, Ooto S, Curcio CA. Subretinal drusenoid deposits a.k.a. pseudodrusen. *Surv Ophthalmol*. 2018;63:782–815.
31. Oak ASW, Messinger JD, Curcio CA. Subretinal drusenoid deposits: further characterization by lipid histochemistry. *Retina*. 2014;34:825–826.
32. Greferath U, Guymer RH, Vessey KA, Brassington K, Fletcher EL. Correlation of histologic features with in vivo imaging of reticular pseudodrusen. *Ophthalmology*. 2016;123:1320–1331.
33. Curcio CA, Messinger JD, Sloan KR, McGwin G, Jr, Medeiros NE, Spaide RF. Subretinal drusenoid deposits in non-neovascular age-related macular degeneration: morphology, prevalence, topography, and biogenesis model. *Retina*. 2013;33:265–276.
34. Steinberg JS, Auge J, Jaffe GJ, et al. Longitudinal analysis of reticular drusen associated with geographic atrophy in age-related macular degeneration. *Invest Ophthalmol Vis Sci*. 2013;54:4054–4060.
35. Curcio CA, Sloan KR, Kalina RE, Hendrickson AE. Human photoreceptor topography. *J Comp Neurol*. 1990;292:497–523.
36. Guyton JR, Klemp KF. Ultrastructural discrimination of lipid droplets and vesicles in atherosclerosis: value of osmium-thiocarbohydrazide-osmium and tannic acid-paraphenylenediamine techniques. *J Histochem Cytochem*. 1988;36:1319–1328.
37. Curcio CA, Millican CL, Allen KA, Kalina RE. Aging of the human photoreceptor mosaic: evidence for selective vulnerability of rods in central retina. *Invest Ophthalmol Vis Sci*. 1993;34:3278–3296.
38. Sura AA, Chen L, Messinger JD, et al. Measuring the contributions of basal laminar deposit and Bruch's membrane in age-related macular degeneration. *Invest Ophthalmol Vis Sci*. 2020;61(13):19.
39. Curcio CA, Messinger JD, Mitra AM, Sloan KR, McGwin G, Jr, Spaide R. Human chorioretinal layer thicknesses measured using macula-wide high resolution histological sections. *Invest Ophthalmol Vis Sci*. 2011;52:3943–3954
40. Li M, Dolz-Marco R, Huisingh C, et al. Clinicopathologic correlation of geographic atrophy secondary to age-related macular degeneration. *Retina*. 2019;39:802–816.
41. Li M, Dolz-Marco R, Messinger JD, et al. Clinicopathologic correlation of aneurysmal type 1 neovascularization in age-related macular degeneration. *Ophthalmology Retina*. 2019;3:99–111.
42. Zanzottera EC, Messinger JD, Ach T, Smith RT, Curcio CA. Subducted and melanotic cells in advanced age-related macular degeneration are derived from retinal pigment epithelium. *Invest Ophthalmol Vis Sci*. 2015;56:3269–3278.
43. Zanzottera EC, Messinger JD, Ach T, Smith RT, Freund KB, Curcio CA. The Project MACULA retinal pigment epithelium grading system for histology and optical coherence tomography in age-related macular degeneration. *Invest Ophthalmol Vis Sci*. 2015;56:3253–3268.
44. Diabetic Retinopathy Study. Report Number 6. Design, methods, and baseline results. Report Number 7. A modification of the Airlie House classification of diabetic retinopathy. Prepared by the Diabetic Retinopathy. *Invest Ophthalmol Vis Sci*. 1981;21:1–226.
45. Yehoshua Z, Wang F, Rosenfeld PJ, Penha FM, Feuer WJ, Gregori G. Natural history of drusen morphology in age-related macular degeneration using spectral domain optical coherence tomography. *Ophthalmology*. 2011;118:2434–2441.
46. Li M, Dolz-Marco R, Messinger JD, et al. Clinicopathologic correlation of anti-vascular endothelial growth factor-treated type 3 neovascularization in age-related macular degeneration. *Ophthalmology*. 2018;125:276–287.
47. Mehta N, Chong J, Tsui E, et al. Presumed foveal bacillary layer detachment in a patient with toxoplasmosis chorioretinitis and pachychoroid disease [published online ahead of print August 26, 2018]. *Retin Cases Brief Rep*, doi:10.1097/ICB.0000000000000817.
48. Curcio CA, Millican CL. Basal linear deposit and large drusen are specific for early age-related maculopathy. *Arch Ophthalmol*. 1999;117:329–339.
49. Sarks JP, Sarks SH, Killingsworth MC. Morphology of early choroidal neovascularisation in age-related macular degeneration: correlation with activity. *Eye (Lond)*. 1997;11(pt 4):515–522.
50. Rudolf M, Clark ME, Chimento M, Li C-M, Medeiros NE, Curcio CA. Prevalence and morphology of druse types in the macula and periphery of eyes with age-related maculopathy. *Invest Ophthalmol Vis Sci*. 2008;49:1200–1209.
51. Green WR, Enger C. Age-related macular degeneration histopathologic studies: the 1992 Lorenz E. Zimmerman Lecture. *Ophthalmology*. 1993;100:1519–1535.
52. Curcio CA, Messinger JD, Sloan KR, McGwin G, Medeiros NE, Spaide RF. Subretinal drusenoid deposits in non-neovascular age-related macular degeneration:

Investigative Ophthalmology & Visual Science

morphology, prevalence, topography, and biogenesis model. *Retina*. 2013;33:265–276.
53. Friedman E, Smith TR. Clinical and pathological study of choroidal lipid globules. *Arch Ophthalmol*. 1966;75:334–336.
54. Dolz-Marco R, Glover JP, Litts KM, et al. Choroidal and sub-retinal pigment epithelium caverns: multimodal imaging and correspondence with Friedman lipid globules. *Ophthalmology*. 2018;125:1287–1301.
55. Spaide RF, Curcio CA. Drusen characterization with multimodal imaging. *Retina*. 2010;30:1441–1454.
56. Chen L, Messinger JD, Zhang Y, Spaide RF, Freund KB, Curcio CA. Subretinal drusenoid deposit in age-related macular degeneration: histologic insights into initiation, progression to atrophy, and imaging. *Retina*. 2020;40:618–631.
57. Chen L, Messinger JD, Sloan KR, et al. Non-exudative neovascularization supporting outer retina in age-related macular degeneration, a clinicopathologic correlation. *Ophthalmology*. 2020;127:931–947.
58. Grossniklaus HE, Miskala PH, Green WR, et al. Histopathologic and ultrastructural features of surgically excised subfoveal choroidal neovascular lesions: Submacular Surgery Trials Report No. 7. *Arch Ophthalmol*. 2005;123:914–921.
59. Spaide RF, Armstrong D, Browne R. Continuing medical education review: choroidal neovascularization in age-related macular degeneration—what is the cause? *Retina*. 2003;23:595–614.
60. Cohen SY, Creuzot-Garcher C, Darmon J, et al. Types of choroidal neovascularisation in newly diagnosed exudative age-related macular degeneration. *Br J Ophthalmol*. 2007;91:1173–1176.
61. Jung JJ, Chen CY, Mrejen S, et al. The incidence of neovascular subtypes in newly diagnosed neovascular age-related macular degeneration. *Am J Ophthalmol*. 2014;158:769–779.e762.
62. Bressler SB, Bressler NM, Fine SL, McCormick P, Auer C. Subfoveal neovascular membranes in senile macular degeneration: relationship between membrane size and visual prognosis. *Retina*. 1983;3:7–11.
63. Zeng G, Taylor SM, McColm JR, et al. Orientation of endothelial cell division is regulated by VEGF signaling during blood vessel formation. *Blood*. 2007;109:1345–1352.
64. Mullins RF, Johnson MN, Faidley EA, Skeie JM, Huang J. Choriocapillaris vascular dropout related to density of drusen in human eyes with early age-related macular degeneration. *Invest Ophthalmol Vis Sci*. 2011;52:1606–1612.
65. Yi K, Mujat M, Park BH, et al. Spectral domain optical coherence tomography for quantitative evaluation of drusen and associated structural changes in non-neovascular age-related macular degeneration. *Br J Ophthalmol*. 2009;93:176–181.
66. Gregori G, Wang F, Rosenfeld PJ, et al. Spectral domain optical coherence tomography imaging of drusen in nonexudative age-related macular degeneration. *Ophthalmology*. 2011;118:1373–1379.
67. Freeman SR, Kozak I, Cheng L, et al. Optical coherence tomography-raster scanning and manual segmentation in determining drusen volume in age-related macular degeneration. *Retina*. 2010;30:431–435.
68. Garcia Filho CA, Yehoshua Z, Gregori G, et al. Change in drusen volume as a novel clinical trial endpoint for the study of complement inhibition in age-related macular degeneration. *Ophthalmic Surg Lasers Imaging Retina*. 2014;45:18–31.
69. Lei J, Balasubramanian S, Abdelfattah NS, Nittala M, Sadda SR. Proposal of a simple optical coherence tomography-based scoring system for progression of age related macular degeneration. *Graefes Arch Clin Exp Ophthalmol*. 2017;255:1551–1558.
70. Corvi F, Srinivas S, Nittala MG, et al. Reproducibility of qualitative assessment of drusen volume in eyes with age related macular degeneration [published online ahead of print November 19, 2020]. *Eye (Lond)*, doi:10.1038/s41433-020-01293-0.
71. Curcio CA. Soft drusen in age-related macular degeneration: biology and targeting via the oil spill strategies. *Invest Ophthalmol Vis Sci*. 2018;59:AMD160–AMD181.
72. Thomas SE, Harrison EH. Mechanisms of selective delivery of xanthophylls to retinal pigment epithelial cells by human lipoproteins. *J Lipid Res*. 2016;57:1865–1878.
73. Vachali PP, Besch BM, Gonzalez-Fernandez F, Bernstein PS. Carotenoids as possible interphotoreceptor retinoid-binding protein (IRBP) ligands: a surface plasmon resonance (SPR) based study. *Arch Biochem Biophys*. 2013;539:181–186.
74. Pollreisz A, Reiter GS, Bogunovic H, et al. Topographic distribution and progression of soft drusen in age-related macular degeneration implicate neurobiology of the fovea. *Invest Ophthalmol Vis Sci*. 2021;61:2356.
75. Owsley C, McGwin G, Jr, Clark ME, et al. Delayed rod-mediated dark adaptation is a functional biomarker for incident early age-related macular degeneration. *Ophthalmology*. 2016;123:344–351.
76. Lee AY, Wu Y, Spaide T, et al. Exploring a structural basis for delayed rod-mediated dark adaptation in age-related macular degeneration via deep learning. *Transl Vis Sci Technol*. 2020;9(2):62.
77. Burgess S, Davey Smith G. Mendelian randomization implicates high-density lipoprotein cholesterol-associated mechanisms in etiology of age-related macular degeneration. *Ophthalmology*. 2017;124:1165–1174.
78. Fritsche LG, Igl W, Bailey JN, et al. A large genome-wide association study of age-related macular degeneration highlights contributions of rare and common variants. *Nat Genet*. 2016;48:134–143.
79. Zarubina AV, Neely DC, Clark ME, et al. Prevalence of subretinal drusenoid deposits in older persons with and without age-related macular degeneration, by multimodal imaging. *Ophthalmology*. 2016;123:1090–1100.
80. Haj Najeeb B, Deak G, Schmidt-Erfurth U, Gerendas BS. The RAP study, report two: the regional distribution of macular neovascularization type 3, a novel insight into its etiology. *Retina*. 2020;40(12):2255–2262.
81. Kim JH, Chang YS, Kim JW, Kim CG, Lee DW. Characteristics of type 3 neovascularization lesions: focus on the incidence of multifocal lesions and the distribution of lesion location. *Retina*. 2020;40:1124–1131.
82. Curcio CA, Presley JB, Malek G, Medeiros NE, Avery DV, Kruth HS. Esterified and unesterified cholesterol in drusen and basal deposits of eyes with age-related maculopathy. *Exp Eye Res*. 2005;81:731–741.
83. Rudolf M, Malek G, Messinger JD, Wang L, Clark ME, Curcio CA. Sub-retinal drusenoid deposits in human retina: organization and composition. *Exp Eye Res*. 2008;87:402–408.
84. Ebrahimi KB, Fijalkowski N, Cano M, Handa JT. Decreased membrane complement regulators in the retinal pigmented epithelium contributes to age-related macular degeneration. *J Pathol*. 2013;229:729–742.
85. Pilgrim MG, Lengyel I, Lanzirotti A, et al. Sub-retinal pigment epithelial deposition of drusen components including hydroxyapatite in a primary cell culture model. *Invest Ophthalmol Vis Sci*. 2017;58:708–719.
86. Spaide RF. Improving the age-related macular degeneration construct: a new classification system. *Retina*. 2017;38:891–899.

Investigative Ophthalmology & Visual Science

87. Chen L, Zhang X, Liu B, Mi L, Wen F. Age-related scattered hypofluorescent spots on late-phase indocyanine green angiography: the multimodal imaging and relevant factors. *Clin Exp Ophthalmol*. 2018;46:908–915.
88. Chong SP, Zhang T, Kho A, Bernucci MT, Dubra A, Srinivasan VJ. Ultrahigh resolution retinal imaging by visible light OCT with longitudinal achromatization. *Biomed Opt Express*. 2018;9:1477–1491.
89. Tong Y, Ben Ami T, Hong S, et al. Hyperspectral autofluorescence imaging of drusen and retinal pigment epithelium in donor eyes with age-related macular degeneration. *Retina*. 2016;36(Suppl):S127–S136.
90. Arnold JJ, Quaranta M, Soubrane G, Sarks SH, Coscas G. Indocyanine green angiography of drusen. *Am J Ophthalmol*. 1997;124:344–356.
91. Chen L, Zhang X, Li M, Gan Y, Wen F. Drusen and age-related scattered hypofluorescent spots on late-phase indocyanine green angiography, a candidate correlate of lipid accumulation. *Invest Ophthalmol Vis Sci*. 2018;59:5237–5245.
92. Lee B, Chen S, Moult EM, et al. High-speed, ultrahigh-resolution spectral-domain oct with extended imaging range using reference arm length matching. *Transl Vis Sci Technol*. 2020;9:12.
93. Rudolf M, Clark ME, Chimento MF, Li CM, Medeiros NE, Curcio CA. Prevalence and morphology of druse types in the macula and periphery of eyes with age-related maculopathy. *Invest Ophthalmol Vis Sci*. 2008;49:1200–1209.
94. Anderson DMG, Messinger JD, Patterson NH, et al. The molecular landscape of the human retina and supporting tissues by high resolution imaging mass spectrometry. *J Am Soc Mass Spectrom*. 2020;7/7/20 online, doi:10.1021/jasms.0c00119.
95. Pollreisz A, Neschi M, Sloan KR, et al. An atlas of human retinal pigment epithelium organelles significant for clinical imaging. *Invest Ophthalmol Vis Sci*. 2020;61:13.
96. Zheng W, Mast N, Saadane A, Pikuleva IA. Pathways of cholesterol homeostasis in mouse retina responsive to dietary and pharmacologic treatments. *J Lipid Res*. 2015;56:81–97.
97. Dinculescu A, Min SH, Dyka FM, et al. Pathological effects of mutant C1QTNF5 (S163R) expression in murine retinal pigment epithelium. *Invest Ophthalmol Vis Sci*. 2015;56:6971–6980.
98. Marmorstein LY, McLaughlin PJ, Peachey NS, Sasaki T, Marmorstein AD. Formation and progression of sub-retinal pigment epithelium deposits in Efemp1 mutation knock-in mice: a model for the early pathogenic course of macular degeneration. *Human Molecular Genetics*. 2007;16:2423–2432.
99. Storti F, Klee K, Todorova V, et al. Impaired ABCA1/ABCG1-mediated lipid efflux in the mouse retinal pigment epithelium (RPE) leads to retinal degeneration. *Elife*. 2019;8:e45100.
100. Balaratnasingam C, Yannuzzi LA, Curcio CA, et al. Associations between retinal pigment epithelium and drusen volume changes during the lifecycle of large drusenoid pigment epithelial detachments. *Invest Ophthalmol Vis Sci*. 2016;57:5479–5489.
101. Guymer RH, Rosenfeld PJ, Curcio CA, et al. Incomplete retinal pigment epithelial and outer retinal atrophy (iRORA) in age-related macular degeneration: CAM Report 4. *Ophthalmology*. 2020;127:394–409.
102. Chen L, Messinger JD, Ferrara D, Freund KB, Curcio CA. Stages of drusen-associated atrophy in age-related macular degeneration visible via histologically validated fundus autofluorescence [published online ahead of print November 18, 2020]. *Ophthalmol Retina*, doi:10.1016/j.oret.2020.11.006.
103. Sarks S, Cherepanoff S, Killingsworth M, Sarks J. Relationship of basal laminar deposit and membranous debris to the clinical presentation of early age-related macular degeneration. *Invest Ophthalmol Vis Sci*. 2007;48:968–977.
104. Zhang Y, Wang X, Blanco E, et al. Photoreceptor perturbation around subretinal drusenoid deposits revealed by adaptive optics scanning laser ophthalmoscopy. *Am J Ophthalmol*. 2014;158:584–596.e581.
105. Freund KB, Zweifel SA, Englebert M. Do we need a new classification for choroidal neovascularization in age-related macular degeneration? *Retina*. 2010;30:1333–1349.
106. Spaide RF, Jaffe GJ, Sarraf D, et al. Consensus nomenclature for reporting neovascular age-related macular degeneration data: consensus on neovascular age-related macular degeneration nomenclature study group. *Ophthalmology*. 2019;127:616–636.
107. Yannuzzi LA, Negrao S, Iida T, et al. Retinal angiomatous proliferation in age-related macular degeneration. *Retina*. 2001;21:416–434.
108. Bloom SM, Singal IP. Revised classification of the optical coherence tomography outer retinal bands based on central serous chorioretinopathy analysis. *Retina*. 2021;41(1):181–188.

Investigative Ophthalmology & Visual Science